Available online at www.sciencedirect.com
ScienceDirect
Trans. Nonferrous Met. Soc. China 29(2019) 2027−2034
Transactions of Nonferrous Metals Society of China
www.tnmsc.cn

Microstructures and mechanical properties of BP/7A04 Al matrix composites

Cai-he FAN[1], Ling OU[1,2], Ze-yi HU[1], Jian-jun YANG[1], Gang CHEN[3], Hong-ge YAN[3]

1. School of Metallurgical and Materials Engineering, Hunan University of Technology, Zhuzhou 412007, China;
2. Jiangsu Key Laboratory of Materials Surface Science and Technology, Changzhou University, Changzhou 213164, China;
3. School of Materials Science and Engineering, Hunan University, Changsha 422004, China

Received 26 December 2018; accepted 21 June 2019

Abstract: The microstructures and interface structures of basalt particle reinforced 7A04 Al matrix composites (BP/7A04 Al) were analyzed by using OM, TEM, SEM and EDS, and the mechanical properties of 7A04 Al alloy were compared with those of BP/7A04 Al matrix composites. The results show that the basalt particles are dispersed in the Al matrix and form a strong bonding interface with the Al matrix. SiO_2 at the edge of the basalt particles is continuously replaced by Al_2O_3 formed in the reaction, forming a high-temperature reaction layer with a thickness of several tens of nanometers, and Al_2O_3 strengthens the bonding interface between basalt particles and Al matrix. The dispersed basalt particles promote the dislocation multiplication, vacancy formation and precipitation of the matrix, and the precipitated phases mainly consist of plate-like η ($MgZn_2$) phase and bright white band-shaped or ellipsoidal T ($Al_2Mg_3Zn_3$) phase. The bonding interface, high dislocation density and dispersion strengthening phase significantly improve the mechanical properties of the composites. The yield strength and ultimate tensile strength of BP/7A04 Al matrix composites are up to 665 and 699 MPa, which increase by 11.4% and 10.9% respectively compared with 7A04 Al alloy without basalt particles.

Key words: Al matrix composites; basalt particle; interface structure; precipitated phase; strengthening mechanism

1 Introduction

Basalt resources are rich and basalt can be naturally degraded to soil parent material, so it is an environmentally friendly material. The basalt fiber has the advantages of high strength, excellent wear resistance and chemical stability, so it has been used to prepare resin matrix composites with excellent performance [1−4]. There are also many reports on the application of friction materials, thermal insulation materials, building materials and decorative materials [5−9]. Especially in recent years, the use of basalt fiber to prepare metal matrix composites has also been explored [10−14]. AKHLAGHI et al [10] studied the thermal behavior of fibers in basalt fiber reinforced metal matrix composites and found that the material strength decreased significantly with the increase of temperature and fiber exposure time. VANNAN and VIZHIAN [11,12] found that pressure impregnation is an ideal method for the preparation of basalt fiber reinforced Al matrix composites, but as the fiber volume fraction increases, the ductility of the composites decreases significantly. KARTHIGEYAN et al [13] found that copper plating on the surface of basalt short fibers can improve the bonding between the basalt fiber and the matrix. XIE et al [14] prepared a basalt fiber reinforced Al matrix composites by pressure infiltration method, then analyzed the main reaction between the basalt fiber and the Al matrix. In addition, the effect of the reaction layer on the interfacial bonding strength was analyzed. In conclusion, the existing researches mainly focus on basalt fiber reinforced metal matrix composites, and studies on basalt particle reinforced metal matrix composites have not been reported.

In this work, the BP/7A04 Al matrix composites were prepared by spray forming technology. The effects of basalt particles on the microstructure, interface structure and mechanical properties of Al matrix were studied. The strengthening mechanism of basalt particles

Foundation item: Projects (2019JJ60050, 2018JJ3121) supported by the Natural Science Foundation of Hunan Province, China; Project (KFBM20170004) supported by the Jiangsu Province Key Laboratory of Materials Surface Science and Technology, China
Corresponding author: Ling OU; Tel: +86-731-22183432; E-mail: ouling24@126.com
DOI: 10.1016/S1003-6326(19)65109-5

in Al matrix was discussed in order to lay a theoretical foundation for the industrial application of materials.

2 Experimental

7A04 Al alloy was used as the matrix material, and its chemical composition is Al−6.1Zn−2.4Mg−1.6Cu (wt.%), with the impurity Fe and Si less than 0.2 wt.%. The basalt particles were used as the reinforcing phase and the composition is shown in Table 1. The particle size is between 1 and 10 μm, and its morphology is shown in Fig. 1. The basalt particles selected in this experiment have a density of 2.72 g/cm^3, a service temperature of 13−923 K, and a linear expansion coefficient of 5.5×10^{-6} /K.

Table 1 Composition of basalt particle (wt.%)

SiO_2	Al_2O_3	MgO	CaO	Na_2O	K_2O	TiO_2	Fe_2O_3	FeO
52.06	14.75	6.55	6.77	2.32	1.38	1.08	5.69	8.06

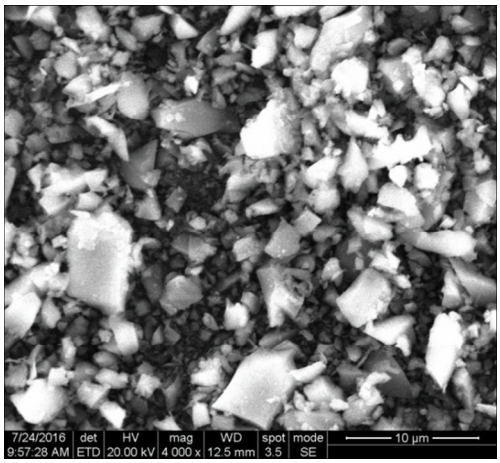

Fig. 1 SEM image of basalt particle

7A04 Al alloy and basalt particle reinforced 7A04 Al alloy composites were prepared on SF380 large-scale injection molding equipment. The Al alloy was smelted in graphite crucible with a melting temperature of 1053 K, and the entire smelting and refining process was protected by anhydrous N_2 to avoid the oxidation of the alloy. Zn, Mg and Cu were added by intermediate alloys Al−40Zn, Al−50Mg and Al−20Cu. When the refining was completed, the temperature was raised to 1103 K, and the molten metal was poured into the preheated graphite crucible through a sealed flow channel. The molten metal in the crucible flew out through a liquid guiding tube with an inner diameter of 3−5 mm, and was fogged in the atomizer. The basalt particles were transported to the atomizer by a quantitative powder feeding device, and the particles were fully mixed with the high pressure N_2 (pressure 0.5−1.5 MPa) in the atomizer. Basalt particles, atomized solid and liquid particles were deposited on a circular iron substrate plate of 100−250 mm away from the atomizer to prepare a basalt granule reinforced Al matrix composites deposited billet with *d*150 mm × 1000 mm, containing 2−5 vol.% of basalt particles. The 7A04 and BP/7A04 Al billets were processed into round ingot of *d*120 mm × 500 mm and extruded into a round bar of *d*30 mm with the extrusion ratio of 16:1 at a temperature of 723 K. The round bar was quenched by solid solution at 733 K for 1.5 h, and its microstructures and mechanical properties were tested after aging at 393 K for 18 h.

The distribution and morphology of the reinforced particles in the Al matrix were observed by M6 optical microscope (OM) and the microstructure of the sample was analyzed by Helios Nanolab 600i scanning electron microscope (SEM) and Titan G2 60-300 transmission electron microscope (TEM). Double-spray electrolysis was carried out after mechanical pre-thinning to about 80 μm. The electrolyte consisted of nitric acid and methanol (volume ratio 1:3) and the temperature was lower than 248 K. The elemental composition of the sample was analyzed using an INCA OXFORD spectrometer. The room temperature tensile properties of the samples were tested on an Instron 3369 stretcher at a draw speed of 1.0 mm/min. Three samples for each variant were investigated. The density of the samples was tested by drainage method.

3 Results

3.1 Microstructures

The metallurgical microstructures of the spray-formed 7A04 Al and BP/7A04 Al-based composites are shown in Fig. 2. It can be seen from Fig. 2(a) that the spray-formed 7A04 Al billet has some pores with the density of 95%, and full density can be achieved after extrusion deformation. There are also a few pores in the Al alloy matrix, as indicated in Fig. 2(b). The basalt particles are dispersed in the Al matrix and no agglomeration of basalt particles is observed. The size of most basalt particles is between 1 and 10 μm, and is consistent with that in the SEM image, which indicates that reinforcing particles with different sizes can be effectively captured and evenly distributed during the spray forming process.

The TEM photographs of the distribution of basalt particles in the matrix of the spray-formed BP/7A04 Al matrix composites are shown in Fig. 3. The basalt particles are well bonded to the matrix interface, and no pores are found at the edge of the basalt particles.

TEM images of the 7A04 Al and BP/7A04 Al-based composites after extrusion and heat treatment are shown in Fig. 4. The microstructures of 7A04 Al alloy and the as-extruded composites are dense and the bonding interface between the reinforcing particles and the matrix

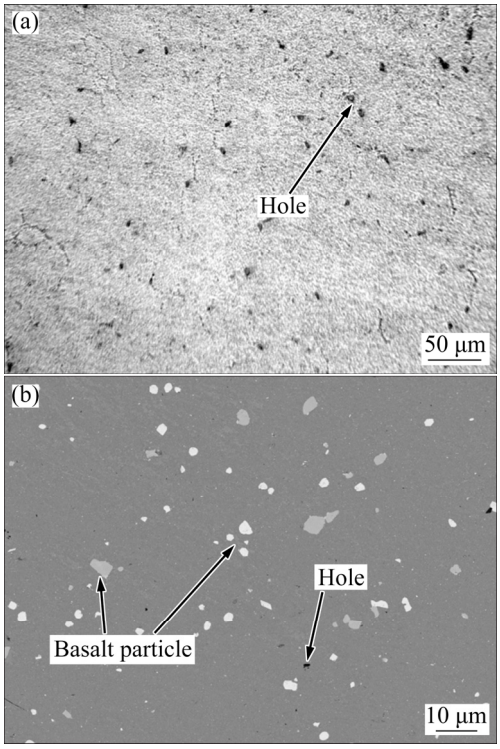

Fig. 2 Metallographic and SEM micrographs of spray-formed 7A04 Al alloy (a) and BP/7A04 Al composites (b)

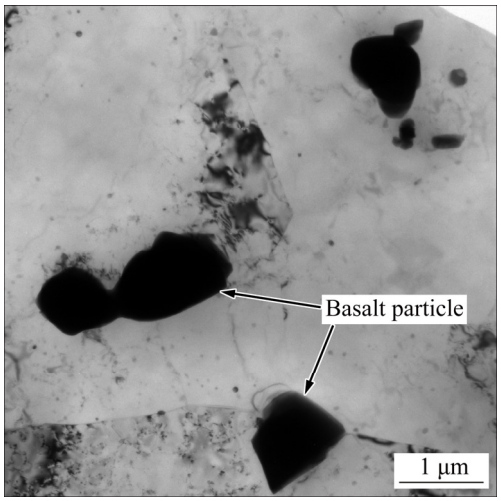

Fig. 3 TEM image of spray-formed BP/7A04 Al composites

is clear and smooth. It can be seen from Fig. 4(a) that there is a certain number of dislocations and η ($MgZn_2$) strengthening phase in as-extruded 7A04 Al alloy, while the dislocations in the heat-treated 7A04 Al matrix basically disappear and the strengthening phase is mainly η phase and T ($Al_2Mg_3Zn_3$) phase (Fig. 4(b)). It can be seen from Fig. 4(c) that there is a large number of

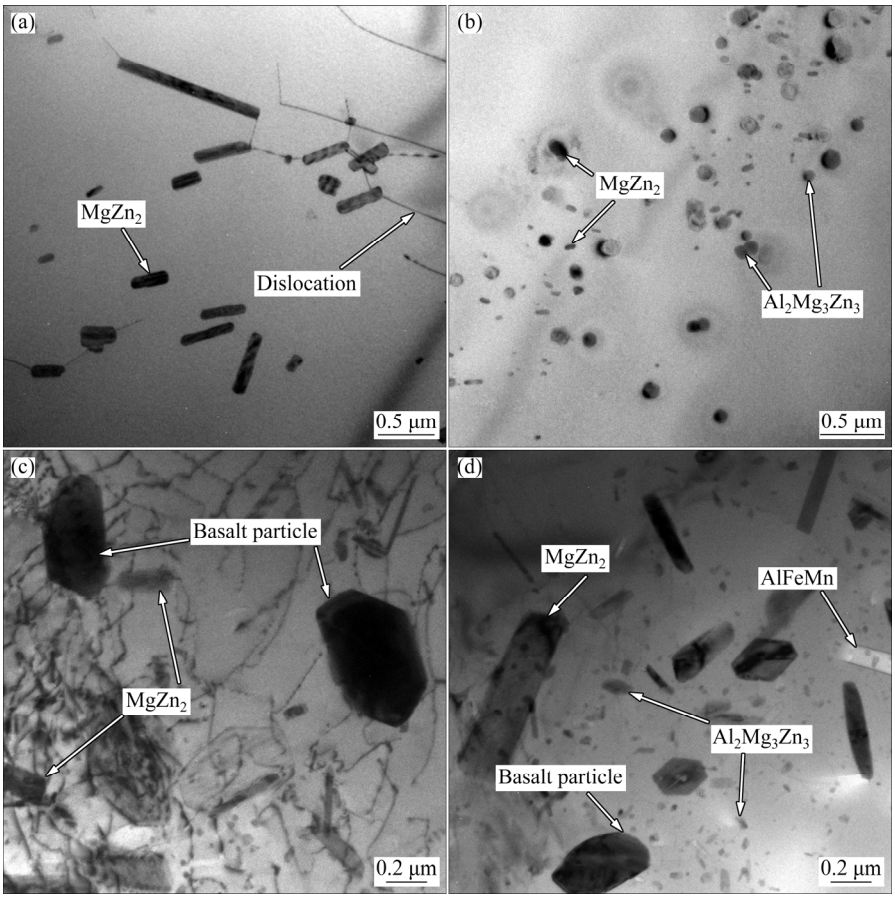

Fig. 4 TEM images of 7A04 Al alloy (a, b) and BP/ 7A04 Al composites (c, d) as-extruded (a, c) and after solid solution and aging (b, d)

dislocations in the extruded BP/7A04 Al matrix composites compared with the extruded 7A04 Al alloy. The dislocation density near the basalt particles is the highest. The precipitated phase in the Al matrix is mainly the plate-like η phase, and the other precipitated phase size is relatively small. After the solid solution aging treatment, the strengthening phases of the extruded BP/7A04 Al composites are mainly plate-like η phases and bright white strip or ellipsoidal T phases, and a small number of impurity phases containing Fe and Si (Fig. 4(d)), such as white strip or block AlFeMn crystal phases and Mg_2Si phases attached to the T phases. Compared with the extruded BP/7A04 Al composites, the dislocation density in the composites after heat treatment significantly reduces, and the size of the η phase significantly increases, mainly because the recovery of the alloy occurs during the solution aging process and the η phase continues to grow.

3.2 Interface structure

TEM images of interface structure between the BP/7A04 Al-based composites and basalt particles are shown in Fig. 5. The basalt particles are strongly embedded at the grain boundaries or intracrystalline of the Al matrix, and do not fall off during the double-spray electrolysis process (Fig. 5(a)). A large number of dislocations can be observed in the Al matrix near the interface. The dislocation source is located at the interface between the reinforcing particles and the Al matrix, and the dislocation density of Al matrix away from the interface is significantly reduced (Fig. 5(b)). In Fig. 5(c), a transition region between the basalt particles and the Al matrix can be clearly observed, the interface between the transition region and the Al matrix is clearly visible. The interface between the Al matrix and the transition zone is not a smooth plane at a higher magnification, but a rough interface, as shown by the curve in Fig. 5(d).

In Fig. 5(c), the EDS analysis results of the 7A04 Al alloy matrix (point *A*), the Al matrix near the interface (point *B*), the transition zone (point *C*), and the basalt particles (point *D*) are shown in Table 2. It can be seen from Table 2 that compared with the Al matrix away from the interface, the content of Si in the Al matrix near the interface slightly increases, the content of other elements does not change much, and the Al matrix

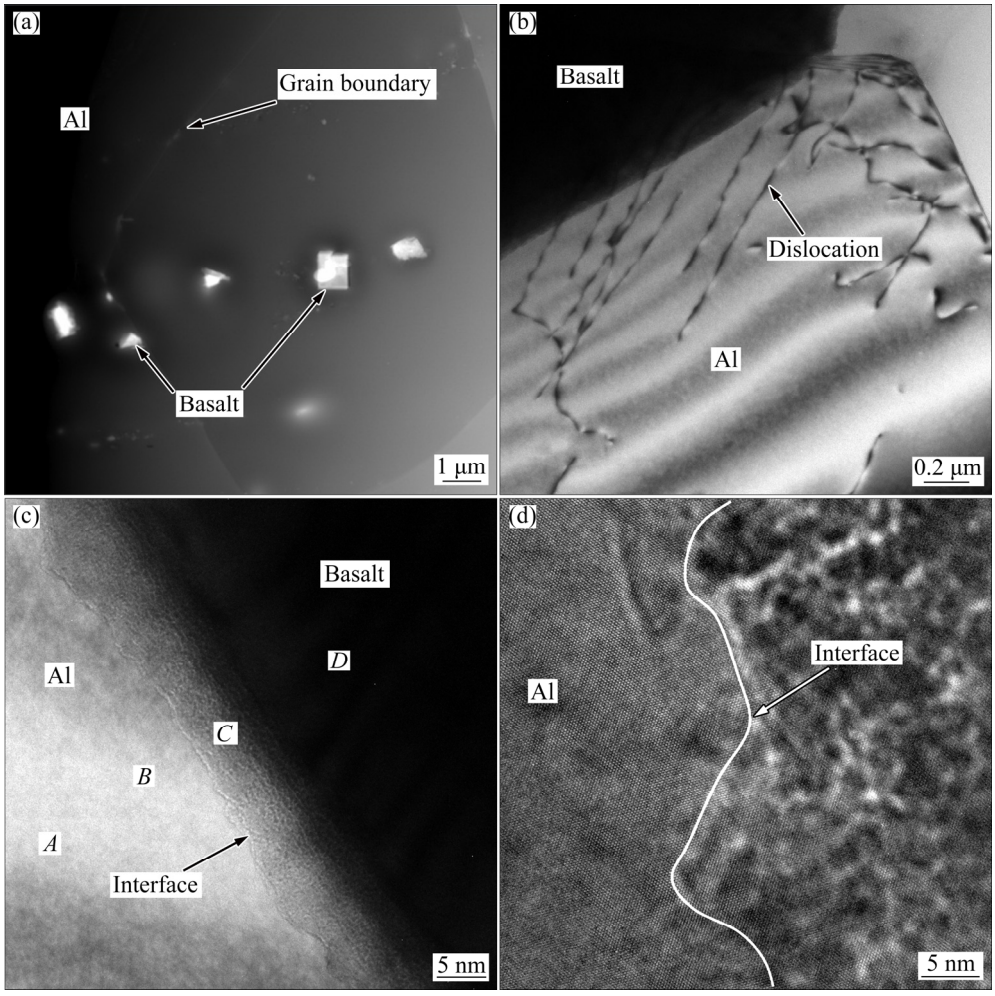

Fig. 5 TEM images of interface between basalt particles and Al matrix of spray-formed BP/7A04 Al composites

Table 2 EDS results of Al alloy matrix, transition zone and basalt particle (at.%)

Element	Point *A*	Point *B*	Point *C*	Point *D*
O	0.12	0.27	58.66	60.65
Na	−	−	1.39	1.28
Mg	3.39	3.31	1.89	1.68
Al	90.15	88.56	10.07	6.15
Si	0.18	1.60	21.88	25.24
K	−	−	0.41	0.52
Ca	−	−	1.71	1.75
Fe	0.10	0.11	2.48	2.51
Zn	4.77	4.90	0.21	0.12
Cu	1.29	1.35	0.12	0.09
Total	100	100	100	100

contains no Na, K and Ca elements. The elemental composition of basalt particles is different from that of the transition area. Compared with the basalt particles, the content of Si in the transition zone significantly decreases, and the content of Al significantly increases.

3.3 Mechanical property

The stress−strain curves of 7A04 Al alloy and BP/7A04 Al matrix composites after solution and aging treatment are shown in Fig. 6. The values of yield strength, ultimate tensile strength and elongation of basalt particle reinforced Al matrix composites are higher than those of 7A04 Al alloy without basalt particles. The yield strength and ultimate tensile strength of 7A04 Al alloy without basalt particles are 597 and 630 MPa, respectively. The yield strength and ultimate tensile strength of BP/ 7A04 Al matrix composites are 665 and 699 MPa, and increase by 11.4% and 10.9%, respectively (Fig. 6(a)).

It can be seen from Fig. 6(b) that the stress−strain curves of two materials near the yield point differ widely. The strain fluctuation of the BP/7A04 Al matrix composites during the yielding stage is small, while the strain of 7A04 Al alloy without basalt particles fluctuates greatly at the same stage. Under the same tensile condition, the beginning yielding time of basalt particle reinforced Al matrix composites during the stretching process is slightly later than that of 7A04 Al alloy without basalt particles, but the stress drop during yielding stage is significantly larger than that of 7A04 Al alloy (Fig. 6(c)).

Fracture morphology micrographs of 7A04 Al alloy and BP/7A04 Al matrix composites after room temperature tensile are shown in Fig. 7. Both of them

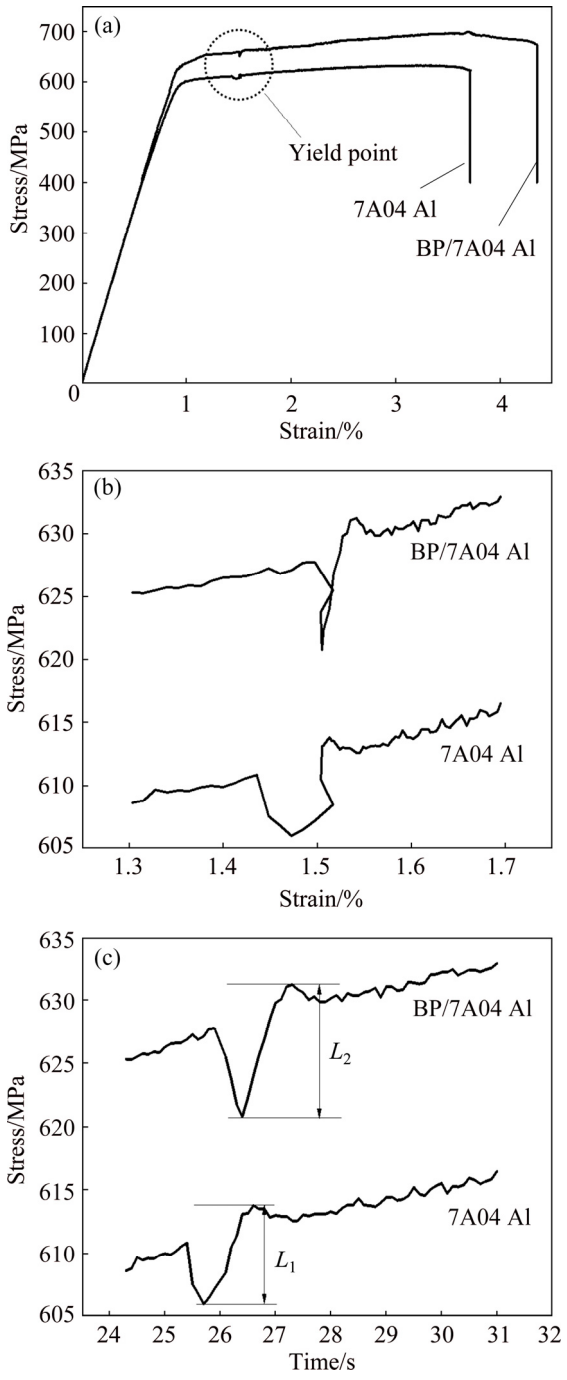

Fig. 6 Stress−strain curves (a, b) and stress−time curves (c) of 7A04 Al alloy and BP/7A04 Al composites after solid solution and aging

exhibit the characteristics of ductile fracture, and a large number of dimples can be observed. No obvious cleavage fracture surface is found, and the tearing rib near the dimple is clearly visible. Compared with Fig. 7(a), the pits can be observed in Fig. 7(b), which are left when the basalt particles are pulled out. A large number of chippings are present in the pits, which are the torn Al matrix during the basalt particle extraction process, as shown in Fig. 7(b).

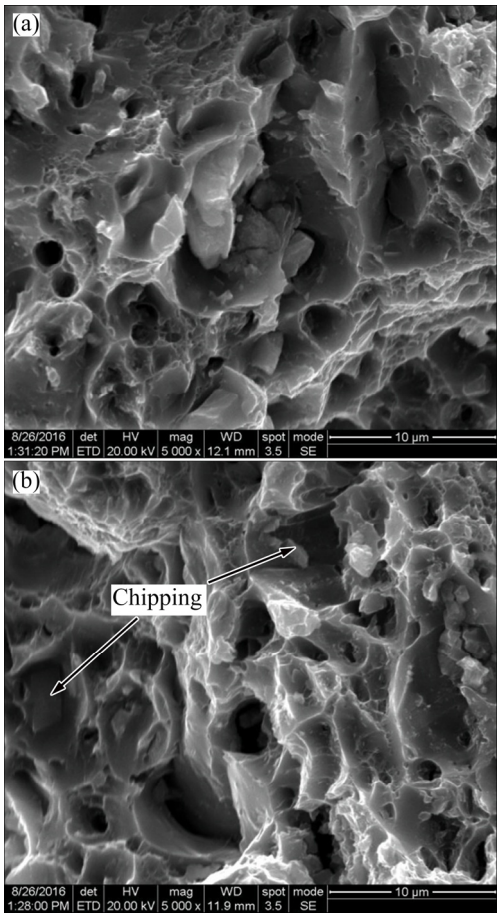

Fig. 7 SEM images of tensile fracture of 7A04 Al alloy (a) and BP/7A04 Al composites (b)

4 Analysis and discussion

4.1 Interface reaction

During the spray forming process, the basalt particles are directly embedded in the atomized droplets or captured by the atomized droplets, and co-deposited into BP/7A04 Al-based composite billets. The reinforcing particles in the composites form a strong bonding interface with the Al matrix (Figs. 3 and 5). The transition zone between basalt particles and Al matrix can be clearly observed in Fig. 5(c). EDS analyses show that the composition of the transition zone is significantly different from the basalt particle center, because SiO_2 which accounts for an absolute majority of the basalt particles composition reacts with the Al matrix near the basalt particles during spray forming and hot extrusion [11]:

$$4Al+3SiO_2=3Si+2Al_2O_3 \quad (1)$$

It can be seen from the formula (1) that SiO_2 in the edge of the basalt particles is continuously replaced by the Al_2O_3 formed by the reaction, resulting in a significant increase of Al element content at the edge of the basalt particles. Although the Si element formed by the reaction does not react with the Al in the matrix, but it can diffuse into the Al matrix under the driving of the gradient, which leads to an increase in the Si content in the Al matrix near the basalt particles, while the Si content in the edge of the basalt particles significantly reduces (Table 2). Previous studies have shown that [8,11], compared with SiO_2, the Al_2O_3 formed by the reaction has better compatibility with the Al matrix, and can form a coherent strong bonding interface. The edge region of the basalt particles is actually a reaction layer with the thickness of several tens of nanometers, and the Al_2O_3 formed by the reaction partially replaces the SiO_2 in the basalt particles. Combined with the experimental results, the existence of this strong coherent bonding surface improves the bonding force between the basalt particles and the Al matrix, resulting in the torn Al near the basalt particles during the stretching process. Some of the chippings that stick to the basalt particles are carried off, and the remainders stay in the pits (Fig. 7(b)). This reaction interface is of great significance for improving the mechanical properties of BP/7A04 Al matrix composites.

4.2 Strengthening mechanism

BP/7A04 Al matrix composites have higher yield strength than 7A04 Al alloys without basalt particles, which is due to the hindrance of dislocation motion caused by basalt particles during tensile deformation. BP/7A04 Al matrix composites prepared by the spray forming process have the dispersion distribution of the reinforced particles in the Al matrix (Fig. 2). Due to the large difference of thermal expansion coefficients between the basalt particles and the base Al alloy, the thermal mismatch stress is generated. Therefore, the composite material is easily subjected to thermal stress and thermal strain on the side of the substrate near the interface after heat treatment, thereby inducing dislocations and deposits at the interface, forming a large number of micro-distortion regions, especially at the sharp corners of the particles. Moreover, the dislocation density is also higher (Fig. 4(c) and Fig. 5(b)). Both the dispersion of the enhanced particles and the rise of the dislocation density in the vicinity increase the hindrance of dislocation motion and contribute to the improvement of the yield strength of the sample [15].

The stress drop on the tensile curve in Fig. 6 corresponds to the process of rapid free movement of dislocations between the reinforcing particles or the second phases after large-scale actuation of microscopic movable dislocations. The stress drop amplitude reflects the pinning ability of the reinforcing particles, the second phase and the Cottrell atmosphere to the dislocation cluster [14,15]. The plastic deformation of the metal conducts by dislocation motion. Compared with the Al

alloy without basalt particles, the BP/7A04 Al matrix composites have more obstacles and greater resistances to dislocation motion. At the same time, diffused distribution of reinforcing particles aggravates the atomic distortion in the nearby Al matrix, and causes the solute atoms to segregate at the extended dislocations, thereby promoting the formation of the Cottrell atmosphere and further increasing the resistance of the dislocation motion. The stress drop of the Al alloy with basalt particles (Fig. 6(c)) is larger than that of the Al alloy without basalt particles (L_2>L_1), which indicates that the basalt particles in the Al matrix not only have strong ability to hinder dislocation motion, but also enhance the pinning ability of the dislocation cluster by promoting the formation of the Cottrell atmosphere, so the yield strength of the sample increases.

The intensity of dynamic strain ageing (DSA) is related to the number of precipitated phases. The more the number of precipitated phases is, the stronger the hindrance effect of dislocation motion is [16]. The micrographs of the precipitates of 7A04 Al alloy and BP/7A04 Al composites after solution treatment and aging treatment are shown in Fig. 8. The morphology and the dimensions of the precipitated phases of two materials are basically the same, but the number of precipitated phases in the BP/7A04 Al matrix composite sample is significantly more than that of the Al alloy without basalt particles. Existing research results found that in SiC/2014 A1 composites, the addition of SiC reinforcing particles causes an increase in thermal mismatch stress of the matrix, so leads to an increase in dislocation density. The high dislocation density promotes the non-uniform nucleation of the metastable phase and contributes to the formation and growth of the precipitation phase [17,18], which is consistent with the findings of this work. Comparing Fig. 4(b) with Fig. 4(d), the size of the precipitated phases in the BP/7A04 Al matrix composite sample is significantly larger than that of the 7A04 Al alloy, mainly because the addition of basalt particles significantly increases the dislocation density of the matrix and promotes the solution during solid solution. The formation of a large number of vacancies accelerates the atomic diffusion rate at the beginning of aging, greatly promotes the nucleation and growth of the precipitated phase, and causes the solute atoms to cluster at a very high speed to form the GP zone.

Study has shown that the enhanced efficiency of reinforcing particles and precipitation contributed to the yield strength increases as the particle size decreases [19]. The thermal expansion coefficients differences among the reinforcing particles lead to the increase of the number and volume of thermal mismatch regions, so the probability of generating geometrically necessary dislocations also greatly increases, and the yield strength increment due to geometrically necessary dislocations is [20]

$$\Delta\sigma = \sqrt{(\Delta\sigma_1)^2 + (\Delta\sigma_2)^2} \quad (2)$$

where $\Delta\sigma_1$ is the yield strength increment caused by thermal mismatch, and $\Delta\sigma_2$ is the yield strength increment caused by mismatch of elastic modulus.

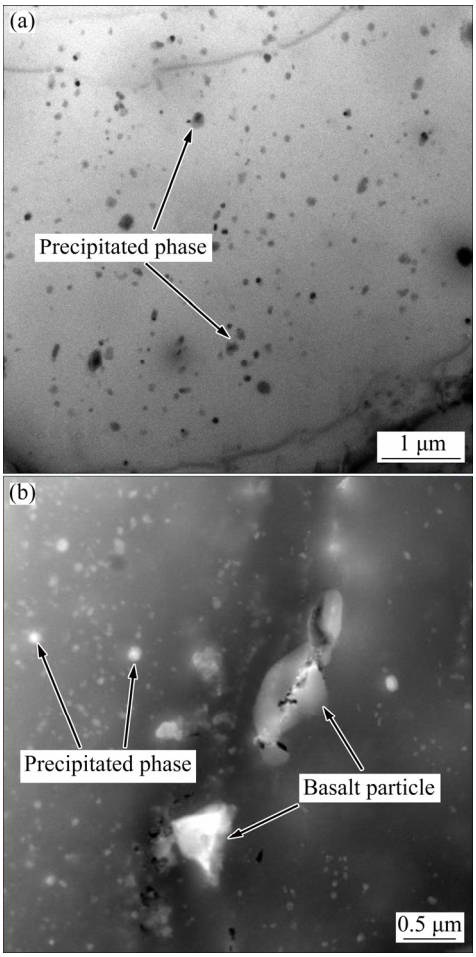

Fig. 8 TEM images of precipitated phase of 7A04 Al alloy (a) and BP/7A04 Al composites (b) after solid solution and aging

5 Conclusions

(1) The yield strength and ultimate tensile strength of BP/7A04 Al matrix composites are up to 665 and 699 MPa, which increase by 11.4% and 10.9% respectively compared with 7A04 Al alloy without basalt particles.

(2) The basalt particles are dispersed in the Al matrix, and react with the Al matrix at high temperature, forming a high-temperature reaction layer with a thickness of several tens of nanometers at the edge. The Al_2O_3 formed by the reaction strengthens the bonding interface between the basalt particles and Al matrix.

(3) The strengthening effect of basalt particles on Al matrix is due to hindering dislocations caused by the movement of basalt particles, promoting the formation of the second phase in the matrix and the dislocation multiplication.

References

[1] FIORE V, SCALICI T, BELLA G. A review on basalt fibre and its composites [J]. Composites Part B, 2015, 74(3): 74−94.

[2] QUAGLIARINI E, MONNI F, LENCI S, BONDIOLI F. Tensile characterization of basalt fibre rods and ropes: A first contribution [J]. Construction and Building Materials, 2012, 34(5): 372−381.

[3] KIM J S, LIM J H, HUH Y. Melt-spinning basalt fibre based on dielectric heating and steady-state process characteristics [J]. Fibers & Polymers, 2013, 14(2): 1148−1157.

[4] DHAND V, MITTAL G, RHEE K Y. A short review on basalt fiber reinforced polymer composites [J]. Composites Part B, 2015, 73(7): 166−180.

[5] OZTURK B, ARSLAN F, OZTURK S. Hot wear properties of ceramic and basalt fiber reinforced hybrid friction materials [J]. Tribology International, 2007, 40(1): 37−48.

[6] WANG Q H, ZHANG X R, PEI X Q. Study on the friction and wear behavior of basalt fabric composites filled with graphite and nano-SiO_2 [J]. Materials & Design, 2010, 31(3): 1403−1409.

[7] CAMPIONE G, MEMDOLA L L, MONACO A. Behavior in compression of concrete cylinders externally wrapped with basalt fibers [J]. Composites Part B, 2015, 69(3): 576−586.

[8] DONG J F, WANG Q Y, GUAN Z W. Material properties of basalt fibre reinforced concrete made with recycled earthquake waste [J]. Construction and Building Materials, 2017, 130(6): 241−251.

[9] LUO X, XU J Y, BAI E L. Study on the effect of basalt fiber on the energy absorption characteristics of porous material [J]. Construction and Building Materials, 2014, 68(2): 384−390.

[10] AKHLAGHI F, ESLAMI F R, SABET S M. Synthesis and characteristics of continuous basalt fibre reinforced aluminum matrix composites [J]. Journal of Composite Materials, 2013, 47(5): 3379−2290.

[11] VANNAN E, VIZHIAN P. Prediction of the elastic properties of short basalt fibre reinforced al alloy metal matrix composites [J]. Journal of Minerals & Materials Characterization & Engineering, 2014, 2(4): 61−70.

[12] VANNAN E, VIZHIAN P, KARTHIGEYAN R. Investigation on the influence of basalt fiber on thermal properties of Al7075/basalt fiber metal matrix composites [J]. Procedia Engineering, 2014, 97(3): 432−438.

[13] KARTHIGEYAN R, EZHIL V S, RANGANATH G, PAUL V S, ANNAMALAI K. Effect of coating parameters on coating morphology of basalt short fibre for reinforcement preparation of Al/basalt metal matrix composites [J]. International Journal of Electrochemical Science, 2013, 8(5): 10138−10149.

[14] XIE Yu-ling, WANG Ming-liang, MA Nai-heng, WANG Hao-wei. Interface reaction and property of basalt fiber reinforced Al-based composites [J]. Foundry Technology, 2013, 34(7): 803−806.

[15] CHEN Gang, WAN Jia, HE Ning, ZHANG Hong-ming, HAN Fei, ZHANG Yu-min. Strengthening mechanisms based on reinforcement distribution uniformity for particle reinforced aluminum matrix composites [J]. Transactions of Nonferrous Metals Society of China, 2018, 28(5): 2395−2400.

[16] FAN Cai-he, YAN Hong-ge, PENG Ying-biao, ZHOU Wei, ZHOU Xing-ling. Microstructures and mechanical properties of spray-forming high magnesium aluminum alloy during large strain hot rolling [J]. The Chinese Journal of Nonferrous Metal, 2017, 27(1): 64−71. (in Chinese)

[17] GAO Weng-li, SU Hai, ZHANG Hui, LIU Hong-bo, WANG Jian-hua. Microstructures and mechanical properties of spray co-deposited SiCp/2024 aluminum matrix composite [J]. The Chinese Journal of Nonferrous Metals, 2010, 20(1): 49−54. (in Chinese)

[18] WANG Zhi-wei, YUAN Yan-bo, ZHENG Rui-xiao, AMEYAMA K, MA Chao-li. Microstructures and mechanical properties of extruded 2024 aluminum alloy reinforced by FeNiCrCoAl3 particles [J]. Transactions of Nonferrous Metals Society of China, 2014, 24(4): 2366−2373.

[19] KOUZELI M, MORTENSEN A. Size dependent strengthening in particle reinforced aluminium [J]. Acta Materialia, 2002, 50(1): 39−51.

[20] LI M, MA K, JIANG L, LAVERNIA E J. Synthesis and mechanical behavior of nanostructured Al 5083/n-TiB2 metal matrix composites [J]. Materials Science and Engineering A, 2016, 656(3): 241−248.

BP/7A04 铝基复合材料的显微组织和力学性能

范才河[1]，欧 玲[1,2]，胡泽艺[1]，阳建君[1]，陈 刚[3]，严红革[3]

1. 湖南工业大学 冶金与材料工程学院，株洲 412007；

2. 常州大学 江苏省材料表面科学与技术重点实验室，常州 213164；

3. 湖南大学 材料科学与工程学院，长沙 422004

摘 要：采用金相显微镜(OM)、透射电镜(TEM)、扫描电镜(SEM)和能谱(EDS)分析玄武岩颗粒增强 7A04 铝基复合材料的显微组织和界面结构，对比研究 7A04 铝合金和 BP/7A04 铝基复合材料的力学性能。研究结果表明：玄武岩颗粒在铝基体中弥散分布，并与铝基体形成强力结合界面，玄武岩颗粒边缘的 SiO_2 不断被反应生成的 Al_2O_3 取代，形成一层几十纳米厚度的高温反应层，反应生成的 Al_2O_3 强化了玄武岩颗粒与铝基体的结合界面；弥散分布的玄武岩颗粒可促进基体中位错增殖、空位形成和析出相的析出，析出相主要以板状的 η ($MgZn_2$)相和亮白色条状或椭球状的 T ($Al_2Mg_3Zn_3$)相为主，结合界面、高位错密度及弥散分布的强化相显著提高复合材料的力学性能，BP/7A04 铝基复合材料的屈服强度和极限拉伸强度分别达到 665 和 699 MPa，与未添加玄武岩颗粒的 7A04 铝合金相比分别提高 11.4%和 10.9%。

关键词：铝基复合材料；玄武岩颗粒；界面结构；析出相；强化机制

(Edited by Xiang-qun LI)